A framework for a large-scale machine tool with long coarse linear axes under closed-loop volumetric error compensation

Soichi Ibaraki, Kohei Yuasa, Naoto Saito, Noriaki Kojima

***Abstract*—A large-scale machine tool is typically very inefficient in size, cost, and energy consumption. Some large parts only have a set of machining features, each of which is within a small local region, and their location should meet position and orientation tolerances. In such a machining application, as a more cost- and energy-effective alternative, this paper presents the concept of a "portable" machine tool, where a small machining platform, with the capability to machine each local machining feature in the required accuracy, is moved by long coarse linear axes. The coarse axes only perform the point-to-point positioning to each machining feature and fixed by servo control during the machining. They do not have sufficient positioning repeatability. To ensure the position/orientation accuracy of each machining feature without having highly repeatable coarse axes, this paper proposes the application of a tracking interferometer to measure all the error motions of coarse axes, and then to perform their compensation. This can be seen as a closed-loop feedback control for coarse axes using the tracking interferometer in the loop. The proposed concept is demonstrated by the experiments with its prototype using a six-DOF robot moved by two coarse linear axes.**

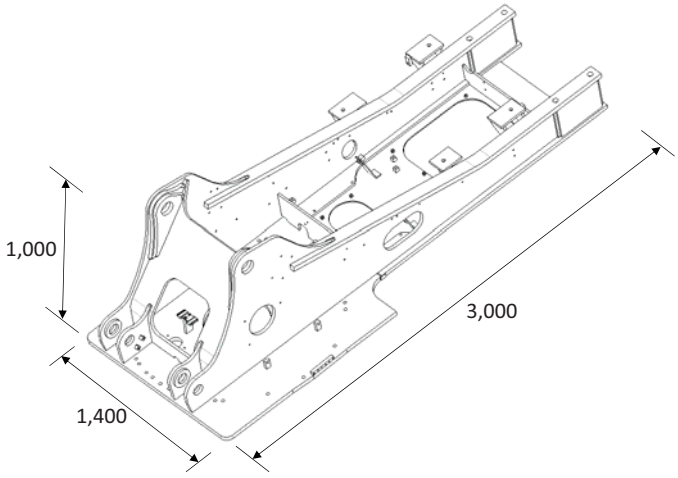

Fig. 1. An example large part (an arm in a large excavator) containing a set of local machining features. Dimensions in millimeters.

I. Introduction

THERE has been a high demand for large and accurate parts in recent "high growth" sectors such as aeronautics, conventional and nuclear power plants, renewable energy power stations, construction machines, railroad, shipping, and large science facilities. Uriarte et al. [1] presented a good review on technological issues with large-scale machine tools. When the part's entire geometry is generated by machining processes (e.g. ribs and spars in an aircraft wing), a large-scale machine tool is indispensable. Some large parts, on the other hand, only have a set of machining features, each of which is within a small local region. For example, an arm part in a large excavator shown in Fig. 1 is produced by the die casting and contains a set of local features that must be machined, such as holes to be drilled or pockets to be end-milled. Their location should meet given position and orientation tolerances. For the part shown in Fig. 1, the position tolerance is typically 0.2 to 0.3 mm.

S. Ibaraki (corresponding author) was with Department of Mechanical Systems Engineering, Hiroshima University, Kagamiyama 1-4-1, Higashi Hiroshima, Hiroshima 739-8527, Japan, e-mail: ibaraki@prec.kyoto-u.ac.jp.

K. Yuasa was with the Department of Micro Engineering, Kyoto University, Katsura, Nishigyo-ku, Kyoto 615-8530, Japan.

N. Saito and N. Kojima were with Komatsu Ltd., 3-1-1 Ueno, Hirakata-shi, Osaka 573-1011, Japan.

Conventional machine tools require a workpiece to be placed inside the machine structure. The size of the complete machine tool system, including backup and ancillary systems, is typically much larger than the size of workpieces. As a result, a large-scale machine tool is generally very inefficient in cost, size, and energy consumption. As a more cost- and energy-effective and flexible alternative, the machine design concept "a small machine for large workpieces" has attracted more attention lately. The review paper [1] calls such a machine a "portable" machine tool and devotes one chapter to its review.

Figure 2 illustrates the concept of a portable machine tool with a coarse linear axis. Each set of local features, holes or a pocket in Fig. 2, is machined by *the machining platform*, with the coarse axis fixed. Features at different locations are machined by moving the machining platform by the coarse axis. Figure 2 depicts a small-sized three-axis machine tool as the machining platform. It can be, alternatively, an industrial serial-link robot (see Fig. 3).

Industrial robots used as a portable machine tool are now commercially available [2], [3]. However, while there are more commercially successful applications of an industrial robot to painting, coating, welding, inspection, deburring, polishing, and so on, there are still fewer applications to milling operations [2]. Its positioning inaccuracy can be a

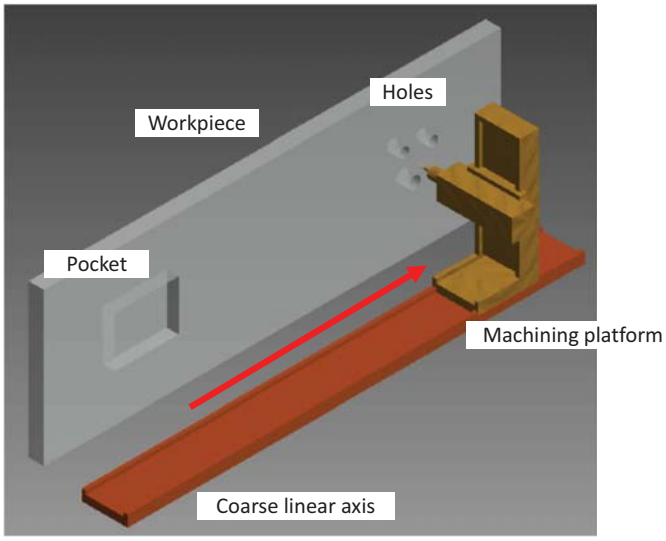

Fig. 2. Concept of a portable machine tool with a coarse linear axis. Each set of local features, holes and a pocket, is machined by the machining platform. The coarse axis is not engaged in the machining operation.

critical issue in milling applications. For a robot to have higher positioning accuracy, the calibration accuracy of its kinematic parameters, e.g. the length of each link, is crucial. They are typically estimated by measuring the end effector's position for a set of given command positions. This is referred to as the *kinematic calibration* of a robot. Its methodologies have been well developed; a review can be found in [4], [5]. Typically, a contact-type probe is used to measure the robot's end effector position with respect to an artefact of the pre-calibrated geometry (typical test procedures are described in ISO 9283:1998 [6]). Since the position measurement is done only at a very limited set of points within the workspace, it is typically difficult to ensure sufficient positioning accuracy over the entire workspace. To measure an end effector's three-dimensional (3D) position at an arbitrary position in the workspace, the application of a tracking interferometer (the term in [7]), or a laser tracker, has been lately reported by many researchers [8]–[16]. A tracking interferometer is a laser interferometer with a mechanism to automatically regulate the laser beam direction to the target retroreflector. Its recent applications are reviewed in [17].

In many industrial robots used as a portable machine tool, a coarse axis is not calibrated at all. For example, the Roptalmu robot [18] is a drilling robot moved on the shop floor by an automated guided vehicle (AGV). The machining operations are done when it is fixed to the tooling structure attached to the workpiece. Therefore, the location of the tooling structure, as well as the repeatability in clamping the robot, is a dominant contributor to the position/orientation accuracy of machined features. Electroimpact's Flex Track [23] moves a drilling robot by a flexible guideway attached to a large workpiece. The robot's position/orientation is determined by measuring a set of reference features on the workpiece by a vision-based sensor. Yang et al. [20] presented a parallel-link legged robot for drilling operations with a capability to move on the shop floor. In these works, the reference to determine the robot's location is needed for every machining operation.

In some portable robots, a coarse axis is also kinematically calibrated, and its positioning accuracy is ensured. Electroimpact [19] presented a robotic drilling machine with a linear slide to enable full coverage of the product. The position error of holes drilled by the robot is reported within ± 0.25 mm. This relatively high accuracy is achieved by the coarse axis with the full-closed loop control using a linear encoder. Faro presented the application of a tracking interferometer to the kinematic calibration a 30.9 feet long linear axis, which moves a robot [24]. It should be emphasized that the kinematic calibration can improve the positioning accuracy of an axis, only when its positioning is sufficiently repeatable. A long coarse axis, built with lower cost, often does not have sufficient repeatability.

A notably unique approach was presented by Wang et al. [21]. A tracking interferometer measures the robot end effector's 3D position, and then its positioning error is cancelled real-time in a feedback control manner. In this paper, this is referred to the *closed-loop compensation* of the 3D positioning error of a robot. It can reduce the positioning error even when the machine is not repeatable at all. Uekita et al. [22] presented an essentially similar real-time compensation for a large-scale lathe, but it is limited only to the straightness error motion of a single linear axis.

To apply the closed-loop compensation in [21] to a portable machine tool, a tracking interferometer needs to continuously measure the end effector's position during machining operations. This may not be feasible in practical machining applications. Cutting fluids or chips may disturb the laser measurement. The laser beam can be blocked by the machine, the workpiece or fixtures. The temperature gradient in the workspace may deteriorate the measurement accuracy. Potential issues will be further discussed in Section IV.

Unlike [21], this paper does not apply the real-time compensation to the machining platform itself. A key issue in the configuration shown in Fig. 2 is that the coarse axis lacks sufficient positioning repeatability. This paper proposes the application of a tracking interferometer to measure all the error motions of coarse axes, and then to perform their compensation by modifying the command position for the machining platform. This can be seen as a closed-loop compensation (calibration) for coarse axes only, using the tracking interferometer in the loop. Also, it can be seen as just an application of the closed-loop compensation in [21] with discrete time instants. This paper's main contribution is in the machine design concept, separating a) the coarse axis under closed-loop compensation with a tracking interferometer in the loop, and b) the machining platform of sufficient positioning repeatability.

In many previous works on robotic machining [25]–[28], it has been recognized that the major challenge in robotic machining is lower stiffness of a robotic arm. This issue is not addressed in this paper at all. This paper only deals with how to move a machining platform to the commanded position accurately without the consideration of machining effect. Section IV will comment on some design issues for the

present concept to be implemented in practical applications.

II. Concept of a Portable Machine Tool with Closed-Loop Controlled Coarse Axes

A. Machine concept

The proposed large-scale machine tool configuration consists of the following subsystems:

1) *A machining platform* must be designed such that it has sufficient workspace, the positioning accuracy, the repeatability, and the rigidity, etc., required to machine every machining feature within geometric tolerances.
2) *Coarse linear axes* move the machine tool to each local feature. Their workspace must cover the entire workpiece. They have neither sufficient positioning accuracy nor repeatability for lower machine cost.

A small-sized machine tool with conventional three orthogonal linear axes can be employed as the machining platform as illustrated in Figure 3(a). It can be, alternatively, an industrial serial-link robot as depicted in Fig. 3(b). It must be emphasized that the basic concept is not limited to the robotic machining.

Each machining feature is machined by the machining platform with coarse axes fixed. The geometric accuracy of each machining feature is, therefore, determined by the machining platform's error motions. Since it has sufficient positioning repeatability, off-line volumetric error compensation can be applied if needed. On the other hand, position and orientation accuracies of each feature are mostly determined by the linear positioning error motion, straightness error motions, and angular error motions of coarse axes (see Fig. 4).

When a linear axis does not have sufficient repeatability, the full-closed loop control with a linear encoder is typically applied (see Fig. 5(a)). A linear encoder only measures the linear positioning error motion, and straightness and angular error motions cannot be compensated for. When the linear axis is very long, a linear encoder may not be available. In this paper, a tracking interferometer is applied to measure the 3D position and orientation of the machining platform.

A tracking interferometer is a laser interferometer with a mechanism to automatically regulate the laser beam direction to the target retroreflector. Figure 6 reviews the principle of 3D position measurement by a tracking interferometer. A laser interferometer, often an absolute distance measurement interferometer, measures the distance to the retroreflector, L, along with the laser beam orientation, θ and ϕ.

The proposed control scheme is illustrated in Fig. 5 (b). This can be seen as a closed-loop feedback control using the tracking interferometer in the loop. It should be emphasized that the compensation for coarse axes is not real-time. The coarse axes move to the given command position without any compensation. Then, their position and orientation are measured by using the tracking interferometer, and are cancelled by modifying the machining platform's command trajectory. Wang et al. in [21] applied a tracking interferometer to the real-time control of a robot, requiring a tracking interferometer measuring the end effector's position all the time in machining operations. This paper applies it to the compensation for coarse axes only. This is more feasible in practical applications, since the tracking interferometer measurement is performed only when the machining platform is moved by coarse axes.

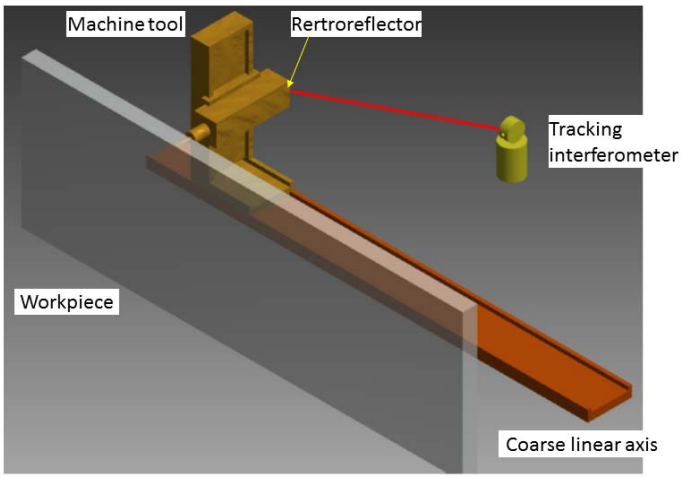

(a)

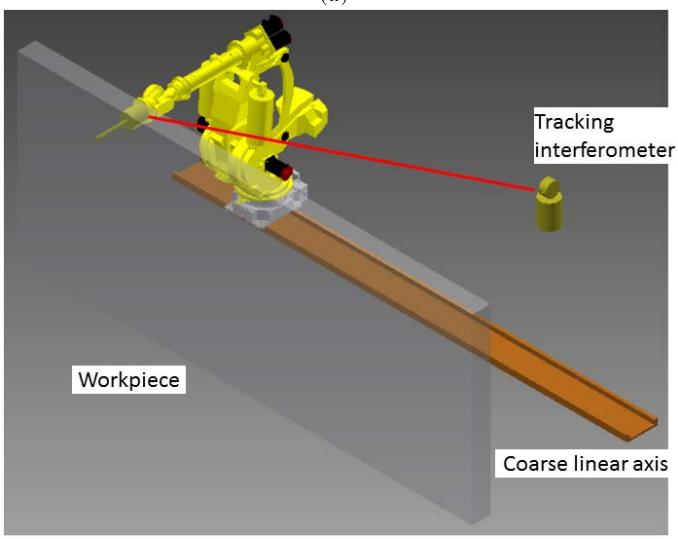

(b)

Fig. 3. Possible configurations of a large-scale machine tool with a long coarse linear axis under closed-loop volumetric error compensation. a) With a small-sized machine tool. b) With a serial-link robot.

This paper targets a machining system with the following specifications:

- The target volumetric accuracy is within 0.3 mm for X, Y and Z position deviations and within 0.1 mm/m for orientation deviations around X, Y and Z axes over the entire workspace.
- The machining platform has a workspace up to $1 \times 1 \times 1$ m. The coarse axes may have the travel up to 10 m.

This target volumetric accuracy can be achieved in many commercial large-sized machine tools. The objective of this paper is to present a compensation scheme for coarse axes that do not have sufficient positioning repeatability.

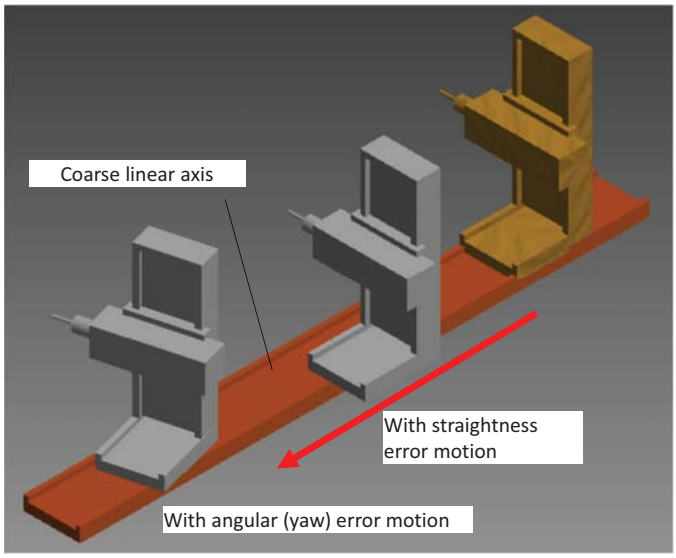

Fig. 4. Influence of error motions of the coarse linear axis on the position and the orientation of the machining platform.

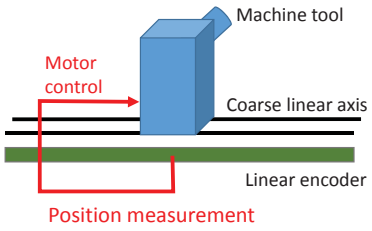

(a) Conventional closed-loop position control by using a linear encoder

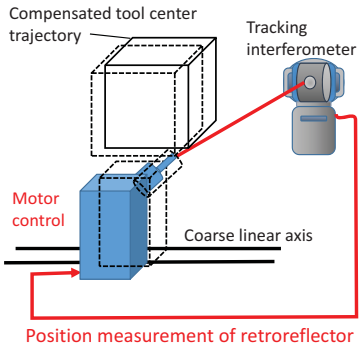

(b) Concept of closed-loop position/orientation control for the coarse linear axis.

Fig. 5. Concept of closed-loop position/orientation control for the coarse linear axis by using a tracking interferometer.

B. Closed-loop compensation for error motions of coarse linear axes

When a coarse linear axis (called the X-axis for example) moves the machining platform to the given command position, $p^* = [a_x, 0, 0]$, it has the linear positioning error motion, E_{XX}, straightness error motions in Y- and Z-directions, E_{YX} and E_{ZX}, as well as angular error motions around X, Y, and Z-directions, E_{AX}, E_{BX}, and E_{CX} (ISO 230-1:2012 [7] defines the terms and the symbols of linear axis error motions). The angular error motions cannot be directly measured by the single point measurement depicted in Fig. 6. When the coarse axis is positioned at the given command position, the retroreflector is positioned at three different points by using the machining platform only, with the coarse axis fixed. Its actual position is measured by using the tracking interferometer. The orientation of the coarse axis can be calculated from them. The detailed algorithm is as follows: define the local coordinate system, ${}^cX - {}^cY - {}^cZ$, attached to the coarse linear axis. It is hereafter referred to as *the coarse axis coordinate system*. Let the machining platform position the retroreflector at three command points in the coarse axis coordinate system, denoted by ${}^cp_0^*$, ${}^cp_1^*$, and ${}^cp_2^* \in \mathbb{R}^3$ (the left-side superscript ^{c} represents a vector in the coarse axis coordinate system). For example, in the experiment to be presented in Section III, command positions are: ${}^cp_0^* = (250, 0, 250)$, ${}^cp_1^* = (-250, 0, 250)$, and ${}^cp_2^* = (250, 250, 250)$ (mm) (see Fig. 9). The retroreflector's actual 3D positions, ${}^rp_0$, ${}^rp_1$, and ${}^rp_2 \in \mathbb{R}^3$, are measured in the global coordinate system by the tracking interferometer. The global coordinate system is attached to the ground and the left-side superscript ^{r} represents a vector in it. The homogeneous transformation matrix (HTM) representing the coordinate transformation from the coarse axis coordinate system to the global coordinate system is given by:

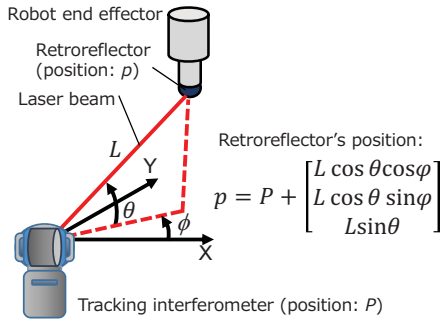

Fig. 6. Principle of position measurement by a tracking interferometer.

$$
\begin{aligned}
{}^rT_c \quad = \quad & D_x(E_{XX})D_y(E_{YX})D_z(E_{ZX})D_a(E_{AX}) \\
& D_b(E_{BX})D_c(E_{CX})D_x(a_x)
\end{aligned} \tag{1}
$$

where $D_x(x)$, $D_y(y)$, and $D_z(z) \in \mathbb{R}^{4\times4}$ are the HTMs representing the translation to the X-, Y-, and Z-directions, respectively. $D_a(a)$, $D_b(b)$, and $D_c(c) \in \mathbb{R}^{4\times4}$ are the HTMs representing the rotation around the X-, Y-, and Z-axes, respectively. They are given by:

$$
D_x(x), D_y(y), D_z(z) = \begin{bmatrix} 1 & 0 & 0 & x \\ 0 & 1 & 0 & y \\ 0 & 0 & 1 & z \\ 0 & 0 & 0 & 1 \end{bmatrix}
$$

$$D_a(\alpha) = \begin{bmatrix} 1 & 0 & 0 & 0 \\ 0 & \cos\alpha & -\sin\alpha & 0 \\ 0 & \sin\alpha & \cos\alpha & 0 \\ 0 & 0 & 0 & 1 \end{bmatrix}$$

$$D_b(\beta) = \begin{bmatrix} \cos\beta & 0 & \sin\beta & 0 \\ 0 & 1 & 0 & 0 \\ -\sin\beta & 0 & \cos\beta & 0 \\ 0 & 0 & 0 & 1 \end{bmatrix},$$

$$D_c(\gamma) = \begin{bmatrix} \cos\gamma & -\sin\gamma & 0 & 0 \\ \sin\gamma & \cos\gamma & 0 & 0 \\ 0 & 0 & 1 & 0 \\ 0 & 0 & 0 & 1 \end{bmatrix} \quad (2)$$

Error motions of the coarse linear axis, $E_{XX}, \cdots, E_{CX}$, can be calculated by solving the following minimization problem:

$$\min_{E_{XX},\cdots,E_{CX}} \sum_{i=0}^{2} \left\| \begin{bmatrix} {}^{r}p_i \\ 1 \end{bmatrix} - {}^{r}T_c \cdot \begin{bmatrix} {}^{c}p_i^* \\ 1 \end{bmatrix} \right\| \quad (3)$$

This problem can be solved by using the least square method, when error motions are sufficiently small. The formulation above does not contain error motions of the machining platform. The machine tool's positioning is required sufficiently repeatable at ${}^{c}p_0^*$, ${}^{c}p_1^*$, and ${}^{c}p_2^*$.

Error motions of the coarse axis are then compensated for by modifying the machining platform's command trajectory. Suppose that the command position for the machining platform is given by ${}^{c}p_i^*$ in the coarse axis coordinate system. Then, the compensated position is given by:

$$\begin{bmatrix} {}^{c}p_i^{\mathrm{comp}} \\ 1 \end{bmatrix} = D_x(-E_{XX}) \cdots D_c(-E_{CX}) \begin{bmatrix} {}^{c}p_i^* \\ 1 \end{bmatrix} \quad (4)$$

The control scheme presented in this paper can be summarized as follows:

- *Coarse linear axes* have neither sufficient positioning accuracy nor repeatability. When they move the machining platform to each local feature, the machining platform's 3D position and orientation errors are measured by using a tracking interferometer. Then, they are compensated by modifying the command trajectory for the machining platform. The machining operation is done by moving the machining platform only, with the coarse axes fixed by servo control.
- *The machining platform* should have sufficient positioning repeatability. Its systematic 3D positioning error can be compensated off-line, if needed. As was reviewed in Section 1, many off-line compensation methodologies have been well developed.

III. A PROTOTYPE: A ROBOT WITH COARSE AXES

A. Experimental setup

The proposed concept is demonstrated by experiments using a 6-DOF robot moved by long coarse linear axes. The experimental setup is shown in Fig. 7. This 6-DOF serial-link robot is conventionally used for the welding of parts in construction machines. The maximum envelop reachable by the robot's end effector is within 3,437 mm × 3,808 mm in the vertical plane, and within a circle of the radius 1,904 mm in the horizontal plane. The positioning resolution at the end effector is 0.01 mm. Its positioning repeatability is, according to the maker's assessment, ±0.08 mm. The robot's detailed specifications can be found in [30]. The systematic positioning error of the robot is not described in its specifications, since it heavily depends on the robot teaching procedure or the robot's kinematic calibration. In our experiment, the robot had at maximum about 10 mm positioning error (the distance from the measured retroreflector position to its nominal position) within 500×500×500 mm (see also Remark in Section III-B). This robot is moved by coarse X- and Y-axes. They are driven by a ball screw and a servo motor. Their strokes are: X1,800 mm × Y 1,000 mm.

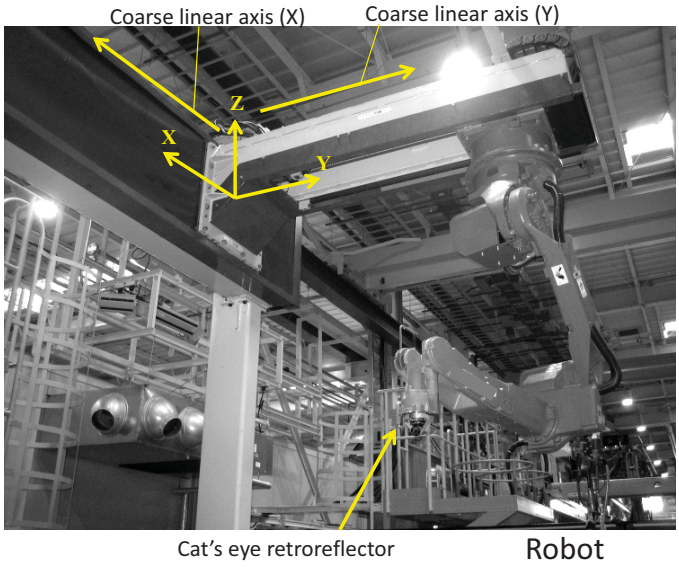

Fig. 7. Experimental setup (the robot moved by coarse linear axes).

This robot was employed in the experiments because it is a good representation of the present machine concept for the following reasons:

- The robot is capable of 6-DOF positioning and its positioning repeatability is more than 10 times higher than that of coarse axes.
- Neither the positioning accuracy nor the repeatability of the coarse X- and Y-axes is sufficiently high.

It should be emphasized that we may not apply this robot to actual machining applications for parts shown in Fig. 1 (the rigidity of the robot may not be sufficient). This prototype is to illustrate the proposed machine concept.

A commercial tracking interferometer, Laser Tracker ION by Faro, was fixed on the floor (see Fig. 8). Table I shows its major specifications [31]. A cat's eye retroreflector is attached to the robot hand. Figure 9 shows test locations of the robot and the tracking interferometer in the XY plane. The coarse axes are positioned at three locations (Locations #1, #2, and #3 in Fig. 9). Then, the robot positions the retroreflector at given total 16 command positions within 500 × 500 × 500 mm, while the coarse axes are fixed at each location.

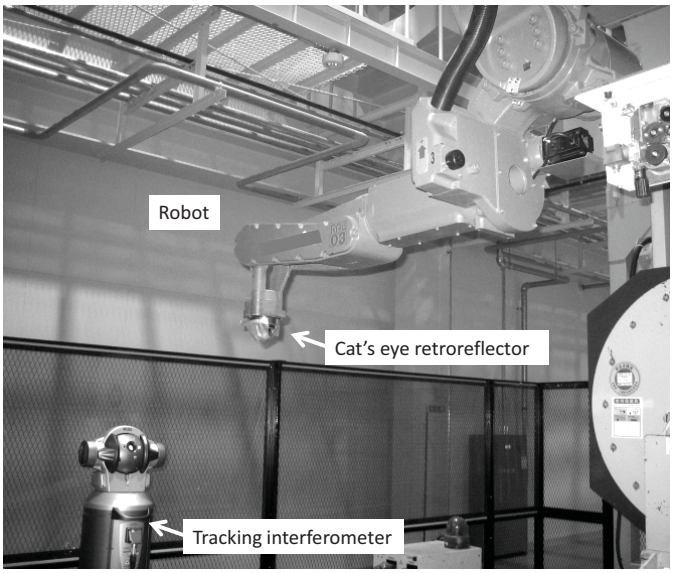

Fig. 8. Experimental setup (the tracking interferometer and the robot).

TABLE I
MAJOR SPECIFICATIONS OF LASER TRACKER ION BY FARO [31]

Laser emission	633-635 nm laser
Range	
Horizontal envelop	$\pm 270^\circ$
Vertical envelop	$+75^\circ$ to -50°
Max working range	30 m (with standard 1/2" SMR)
Distance measurement performance (Agile ADM (Absolute Distance Meter))	
Resolution	0.5 μm
Sample rate	10,000/sec
Accuracy	8μm+0.4μm/m
Angle measurement performance	
Angular accuracy	10μm+2.5μm/m
Max angular velocity	180°/sec

B. Experimental results: Uncompensated end effector positions

In Fig. 10, black markers represent command positions at each coarse axes location ("Location #1" to "#3"). Blue markers show the retroreflector's positions measured by the tracking interferometer. To illustrate the deviation, the error vector from the command point to the measurement point is kept in the same origin and elongated 20 times (see Fig. 11). This error magnification is to more clearly observe position and orientation errors of measured trajectories in the same coordinates for command trajectories. Figure 10(b) shows the projection of Fig. 10(a) onto the XY plane, and Fig. 10(c-1) and (c-2) show its projection onto the YZ plane. Figure 12(a) shows the distance between command and measured positions at each command position.

The global coordinate system is defined based on measured retroreflector positions at Location #1. Therefore, measured positions at Location #1 are not influenced by error motions of coarse axes. Even at Location #1 in Figs. 10 (see also Fig. 12(a)), the retroreflector's position error was at maximum about 10 mm. This is mostly caused by the miscalibration of kinematic parameters of the robot.

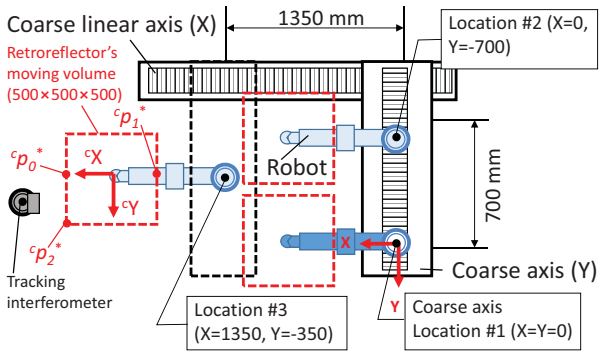

Fig. 9. Test locations in the XY plane. $^cX - ^cY$ represents the coarse axis coordinate system, which moves with the coarse axes. $^cp_0^*$, $^cp_1^*$ and $^cp_2^*$ show the points where error motions of the coarse linear axis, $E_{XX}, \cdots, E_{CX}$, are calculated (see Section II-B).

More importantly, the measured trajectory at Location #3 in Fig. 10(b) is linearly shifted by about 15 mm in the X-direction and about 3 mm in the Y-direction. This shows the influence of the linear positioning error motion and the straightness error motion of the two coarse axes. Furthermore, in Fig. 10(c-1) and (c-2), the measured trajectories at Locations #2 and #3 are tilted around the X-axis. This is caused by the pitch error motion of Y-axis (Locations #2 and #3) and the roll error motion of X-axis (Location #3). The objective of the closed-loop compensation for coarse axes is to reduce these influences.

Table II summarizes orientation and position errors of the coarse axis coordinate system best-fit to the retroreflector's trajectory at each of Locations #1 to #3. They roughly represents position and orientation errors of the coarse axes at each location (there may be some influence by the repeatability error of the robot's positioning). The following observations can be made:

- The positioning error of the coarse axes (X- and Y-axes) was large; at maximum 6.32 mm at Location #3 in the distance to the command position ($\sqrt{\Delta X^2 + \Delta Y^2 + \Delta Z^2}$). The orientation error was also significant. For example, the maximum orientation error, $\Delta A = 1.785$ mm/m at Location #3, changes the retroreflector's position by 0.893 mm at maximum in the Z-direction, since the robot's moving volume was $500 \times 500 \times 500$ mm. Relatively larger ΔZ and ΔA may be attributable to the elastic deformation of the coarse Y-axis rail due to the robot's weight.
- Tests #1 and #2 are the same test done at different days. The difference in $\Delta A, \cdots, \Delta Z$ shows the repeatability error of the coarse axes' positioning. Figure 10 shows measured trajectories in Test #2.

The systematic 3D positioning error of the robot can be compensated off-line. As was reviewed in Section 1, many methodologies have been well developed for off-line compensation. It is not a part of the academic contribution of this paper.

In the experiment, we employed the simplest form of off-line compensation: suppose that the retroreflector's position, ${}^c p_i$, is measured by the tracking interferometer for its command position, ${}^c p_i^*$. Then, the command position is modified from ${}^c p_i^*$ to ${}^c p_i^* - ({}^c p_i - {}^c p_i^*)$. Such a simple compensation may not work when the robot is positioned at a point that is not among a set of pre-calibrated command positions, $\{{}^c p_i^*\}_{i=1,\cdots,N}$.

Remark: The uncompensated positioning error of the robot was significant. For welding applications, in which this robot is originally used, a command trajectory is typically generated by the robotic teaching and the dynamic arc seam tracking is often applied. The robot's systematic volumetric accuracy is, therefore, less important. Furthermore, the positioning error observed at Location #1 may not be caused by the robot only; it may be attributable to the elastic deformation of coarse axes or other auxiliary systems attached to the robot. There is also a contribution of the measurement uncertainty of the tracking interferometer (see Section III-D).

C. Experimental results: under closed-loop compensation for coarse axes

When the coarse axes move to Locations #2 and #3, the compensation presented in Section II-B was applied to their error motions. The objective of the algorithm presented in Section II-B is to calculate the position and the orientation of the coarse axis coordinate system. In this experiment, although the coarse axis coordinate system is moved by the two coarse axes, the same algorithm can be applied. The off-line compensation for the robot (Section III-B) was also applied. Figure 13 shows measured retroreflector positions. Figure 12(b) shows the distance between command and measured positions. In Location #1, the maximum distance error was reduced from about 10 mm (Fig. 12(a)) to about 0.25 mm (Fig. 12(b)). This reduction is mostly attributable to the off-line compensation for the robot. By the closed-loop compensation for coarse axes, it can be observed in Fig. 13 that position and orientation errors of measured trajectories at Locations #2 and #3 are also significantly reduced. The maximum distance between command and measured positions is reduced from about 25 mm (Fig. 12(a)) to 0.65 mm (Fig. 12(b)).

In Fig. 12(a), the error trend looks similar in Locations #1 to #3. This is because this error trend is mostly attributable to the robot's systematic positioning error. When it is compensated in Fig. 12(b), the robot's unrepeatable positioning error becomes the dominant error cause.

Table III summarizes orientation errors (ΔA, ΔB, and ΔC: around X, Y, and Z-axes) and position errors (ΔX, ΔY, ΔZ: in X, Y, and Z directions) of the coarse axis coordinate system best-fit to the retroreflector's trajectory at each of Locations #1 to #3. It compares orientation and position errors of coarse axes (a) without and (b) with the closed-loop compensation. The maximum position error of coarse axes was reduced from -15.6 mm (ΔX at Location #3) to -0.3 mm (ΔX at Location #3). The maximum orientation error was reduced from 1.8 mm/m (ΔA at Location #3) to 0.19 mm/m (ΔB at Location #3).

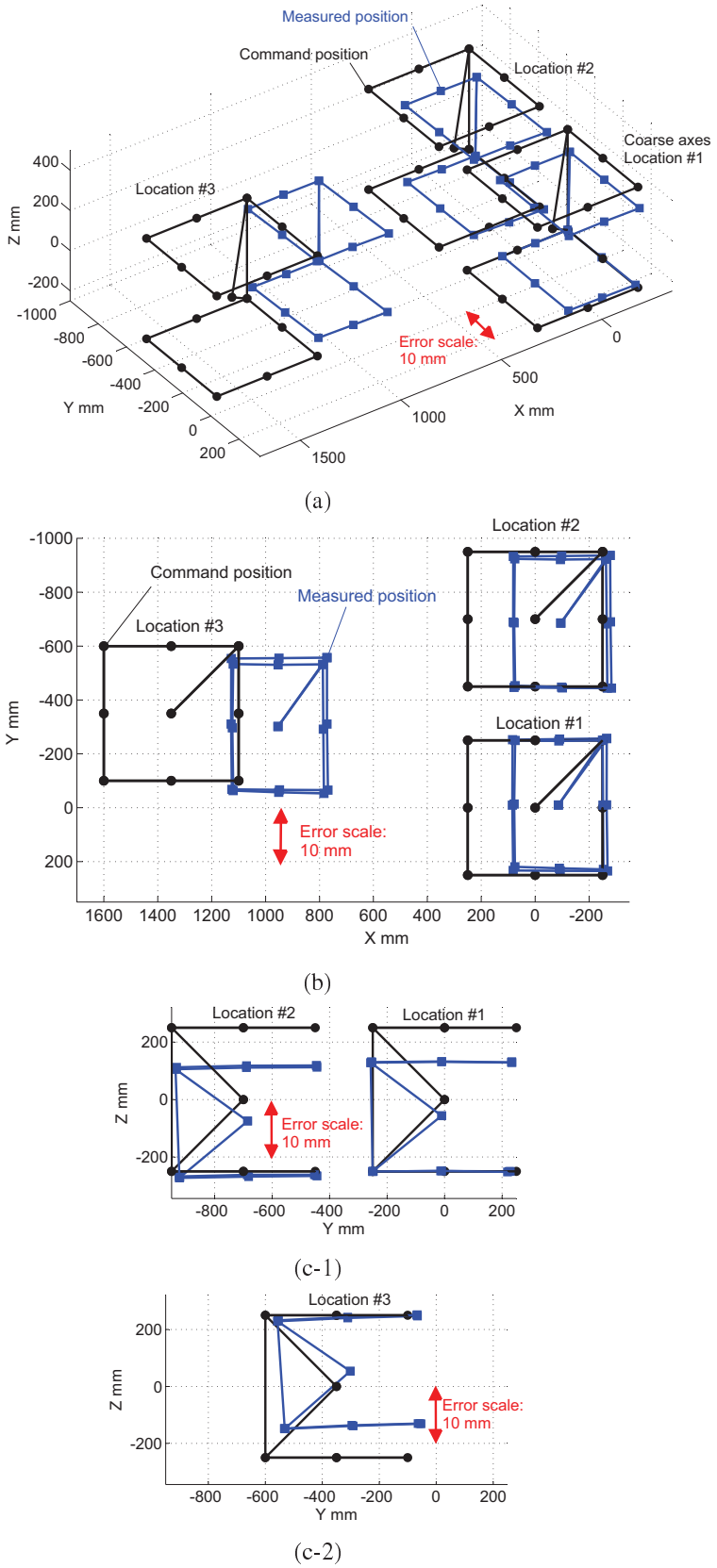

Fig. 10. Retroreflector positions measured by the tracking interferometer (uncompensated). a) In 3D view. b) Projection onto the XY plane. c-1) and c-2) Projection onto the YZ plane. The difference between measured and command positions is magnified 20 times (see Fig. 11).

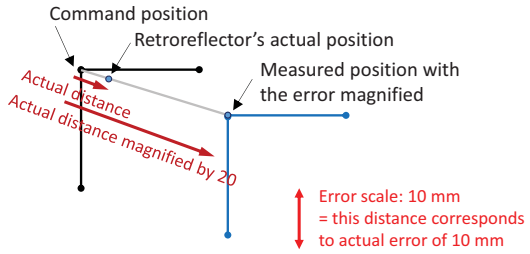

Fig. 11. The magnification of the error in the measured retroreflector position from its command position in Fig. 10.

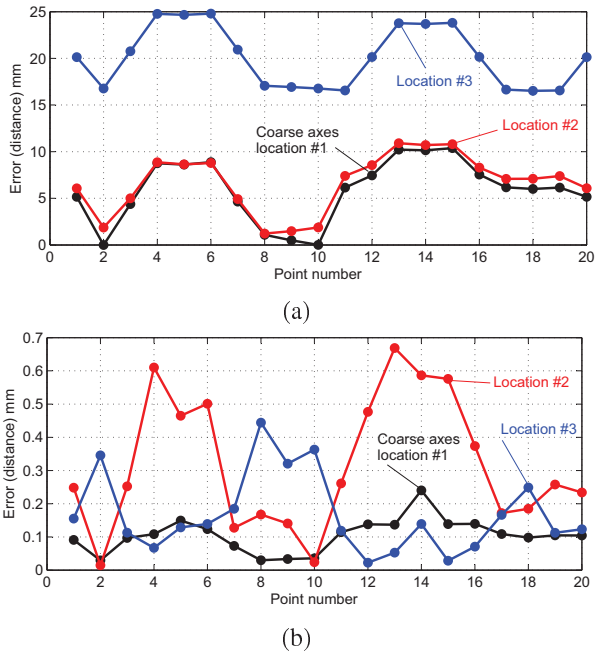

Fig. 12. The distance between command and measured positions of the retroreflector (the horizontal axis represents the index number of each command position). a) Uncompensated. b) Under closed-loop compensation for coarse axes and off-line compensation for the robot's positioning error.

D. Discussion on volumetric error contributors

This subsection briefly discusses contributors to the volumetric error of the present system.

a. Measurement uncertainty of tracking interferometer: The measurement uncertainty of the tracking interferometer is clearly a major contributor. The measurement uncertainty of a tracking interferometer has been studied in many publications [21], [32], [33]. According to Table I, the uncertainty in the retroreflector's position measurement is assessed at maximum 16.5 μm (the distance from the tracking interferometer to the target retroreflector was at maximum 2.6 m in the experiment). Note that this uncertainty does not contain the environmental contribution, e.g. the calibration error of thermal influence on the laser beam wavelength.

Remark: For conventional machine tools or CMMs, the multilateration measurement has been more widely accepted [29], [34], since its measurement uncertainty is typically lower than that of the angular measurement-based approach depicted in Fig. 6. It requires, however, four or more tracking interferometers to simultaneously measure the retroreflector.

b. Positioning error of the robot: The robot's positioning error (both systematic and random) is among major uncertainty contributors. In the experiment, the robot's positioning resolution is 10 μm and its positioning repeatability was, according to the assessment by its maker, $\pm$0.08 mm (see Section III-A) . To achieve the target volumetric accuracy discussed in Section II, this must be further reduced.

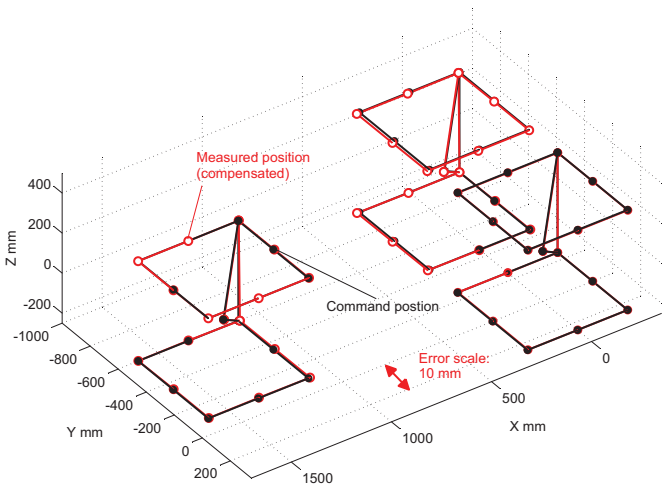

Fig. 13. Retroreflector positions measured by the tracking interferometer, under the closed-loop compensation for coarse axes and off-line compensation of the robot.

TABLE II

ORIENTATION ERRORS (ΔA, ΔB, ΔC: ORIENTATION ERRORS AROUND X, Y, AND Z AXES) AND POSITION ERRORS (ΔX, ΔY, ΔZ: POSITION ERRORS IN X, Y, AND Z DIRECTIONS) OF THE COARSE AXIS COORDINATE SYSTEM BEST-FIT TO THE RETROREFLECTOR'S TRAJECTORY MEASURED BY THE TRACKING INTERFEROMETER AT LOCATIONS #1 TO #3. THEY ROUGHLY REPRESENTS POSITION AND ORIENTATION ERRORS OF THE COARSE AXES AT EACH LOCATION.

Test #1*

	ΔA**	ΔB	ΔC	ΔX	ΔY	ΔZ
Location #1†	0	0	0	0	0	0
Location #2	0.621	0.561	0.088	-0.595	1.595	-1.090
Location #3	1.785	0.027	0.240	-0.448	3.660	5.176

Test #2*

Location #1†	0	0	0	0	0	0
Location #2	0.640	0.462	-0.085	-0.525	1.330	-1.106
Location #3	1.813	0.089	-0.110	-15.566	3.378	5.017

*: Tests #1 and #2 are the same test done at different days. Their difference shows the repeatability error of the coarse axes' positioning.
**: ΔA, ΔB, and ΔC are in mm/m. ΔX, ΔY, and ΔZ are in mm.
†: The global coordinate system is defined according to the retroreflector's trajectory at Location #1.

IV. Design Issues for Practical Implementation

This paper only presents a basic concept to improve the volumetric accuracy of coarse axes. To implement this concept

TABLE III
ORIENTATION ERRORS (ΔA, ΔB, ΔC: AROUND X, Y, AND Z AXES) AND POSITION ERRORS (ΔX, ΔY, ΔZ: IN X, Y, AND Z DIRECTIONS) OF THE COARSE AXIS COORDINATE SYSTEM BEST-FIT TO THE RETROREFLECTOR'S TRAJECTORY WITH AND WITHOUT THE CLOSED-LOOP COMPENSATION.

(a) Without closed-loop compensation for coarse axes

	ΔA^{**}	ΔB	ΔC	ΔX	ΔY	ΔZ
Location #1†	0	0	0	0	0	0
Location #2	0.640	0.462	-0.085	-0.525	1.330	-1.106
Location #3	1.813	0.089	-0.110	-15.566	3.378	5.017

(b) With closed-loop compensation for coarse axes

Location #1†	0	0	0	0	0	0
Location #2	-0.006	0.163	-0.009	0.024	-0.007	0.001
Location #3	0.009	0.189	-0.041	-0.312	0.059	-0.028

**: ΔA, ΔB, and ΔC are in mm/m. ΔX, ΔY, and ΔZ are in mm.
†: The global coordinate system is defined according to the retroreflector's trajectory at Location #1.

in practical applications, many design considerations should be taken into account, which are not covered in this paper. This paper only deals with a scheme to move a machining platform to the commanded position accurately without the consideration of machining effect.

Machine stiffness: As was briefly reviewed in Section I, the major challenge in robotic machining is often lower stiffness of a robotic arm. It must be emphasized that the present compensation scheme for a coarse axis is not restricted to robotic machining. As illustrated in Fig. 3(a), a conventional small machine tool can be employed as a more rigid machining platform. In such a design, the connecting stiffness of the machining platform to the coarse axis, as well as the rigidity of the coarse axis itself, can be crucial.

Influence of chips or cutting fluids: The machining operation is done by moving the machining platform only. When coarse axes move, chips are not generated and thus the tracking interferometer measurement would not be influenced by flying chips. The retroreflector location must be carefully chosen such that the laser beam would not be blocked by the machine, the workpiece, or cutting fluids. The retroreflector does not have to attached close to the tool tip; it should be attached to the linear axis carrying the tool (see Figs.3(a)). The mist from cutting fluids may alter interferometric signals considerably. This requires a good mist extractor for the work chamber.

Location of tracking interferometer: The location of tracking interferometer must be carefully chosen such that the laser beam would not be blocked by the machine or a workpiece within the entire workpiece. It would be crucial to employ a tracking interferometer that can measure the absolute distance to the target (Absolute Distance Meter (ADM)), such that the measurement can be continued even if the laser beam is blocked in a small portion of workspace.

The tracking interferometer should be placed on a separate floor base from the machine, such that its position and orientation would not be affected by the machine's motion. It is also important to note that the tracking interferometer' measurement uncertainty can be significantly different depending on its location relative to the target's workspace.

V. CONCLUSION

The paper presents a control concept for large-scale machine tools. Each machining feature is machined by a small machining platform with coarse axes fixed. Features at different locations are machined by moving the machining platform by coarse linear axes. The closed-loop compensation for error motions of coarse axes is applied based on the 3D position measurement using a tracking interferometer. The validity of the proposed control scheme was investigated by an experiment with a welding robot moved by two coarse linear axes. By applying the closed-compensation for coarse axes using a tracking interferometer, as well as the off-line compensation for the robot's positioning error, the maximum distance between command and measured end effector's positions was reduced from about 25 mm to 0.65 mm. This may contain the measurement uncertainty of the tracking interferometer.

To implement the present closed-loop compensation scheme in industrial applications, many design considerations, as discussed in Section IV, should be taken into account, and it will be further studied in our future development. It is important to note that the measurement uncertainty of the tracking interferometer is clearly one of dominant uncertain factors. Obviously, it cannot be applied to machining applications that require higher accuracy than the tracking interferometer's measurement accuracy.

REFERENCES

[1] L. Uriarte, M. Zatarain, D. Axinte, J. Yagüe-Fabra, S. Ihlenfeldt, J. Eguia, and A. Olarra, "Machine tools for large parts," CIRP Ann Manuf Technol, vol. 62, pp. 731-750, 2013.

[2] Y. Chen and F. Dong, "Robot machining: recent development and future research issues," Int J Adv Manuf Technol, vol. 66, no. 9, pp. 1489-1497, 2013.

[3] I. Iglesias, M. A. Sebastián, and J. E. Ares, "Overview of the State of Robotic Machining: Current Situation and Future Potential," Procedia Engineering, vol. 132, pp. 911-917, 2015.

[4] J. M. Hollerbach and C. W. Wampler, "The calibration index and taxonomy for robot kinematic calibration methods," Int J Robotics Research, vol. 15, no. 6, pp. 573-591, 1996.

[5] Z. S. Roth, B. W. Mooring, and B. Ravani, "An overview of robot calibration," IEEE Trans Robotics and Automation, vol. 3, no. 5, pp. 377-385, 1987.

[6] ISO 9283:1998, Manipulating industrial robots – Performance criteria and related test methods.

[7] ISO 230-1:2012, Test code for machine tools – Part 1: Geometric accuracy of machines operating under no-load or quasi-static conditions.

[8] K. Lau, R. Hocken, and W. Haight, "Automatic laser tracking interferometer system for robot metrology," Prec Eng, vol. 8, no. 1, pp. 3-8, 1986.

[9] M. Vincze, J.P. Prenninger, and H. Gander, "A laser tracking system to measure position and orientation of robot end effectors under motion," Int. J. Robotics Res., vol. 13, no. 4, pp. 305-314, 1994.

[10] C. Gong, J. Yuan, and J. Ni, "Nongeometric error identification and compensation for robotic system by inverse calibration," Int. J. Mach. Tools Manuf., vol. 40, no. 14, pp. 2119-2137, 2000.

[11] G. Alici and B. Shirinzadeh, "A systematic technique to estimate positioning errors for robot accuracy improvement using laser interferometry based sensing," Mechanism and Machine Theory, vol. 40, no. 8, pp. 879-906, 2005.

[12] A. Kohama, R. Mori, S. Komai, M. Suzuki, S. Aoyagi, J. Fujioka, and Y. Kamiya, "Calibration of kinematic parameters of a robot using neural networks by a laser tracking system," Proc. of 7th Int Conf on Machine Automation, pp. 251-256, 2008.

[13] X. D. Ren, Z. R. Feng, and C. P. Su, "A new calibration method for parallel kinematics machine tools using orientation constraint," Int. J. Mach. Tools Manuf., vol. 49, no. 9, pp. 708-721, 2009.
[14] Z. Wang, L. Mastrogiacomo, F. Franceschini, and P. Maropoulos, "Experimental comparison of dynamic tracking performance of iGPS and laser tracker," Int J Adv Manuf Technol, vol. 56, no. 1, pp. 205-213, 2011.
[15] A. Nubiola and I. A. Bonev. "Absolute calibration of an ABB IRB 1600 robot using a laser tracker," Robotics and Computer-Integrated Manufacturing, vol. 29, no. 1, pp.236-245, 2013.
[16] J. F. Wu, R. Zhang, R. H. Wang, and Y. X. Yao, "A systematic optimization approach for the calibration of parallel kinematics machine tools by a laser tracker," Int. J. Mach. Tools Manuf., vol. 86, pp. 1-11, 2014.
[17] B. Muralikrishnan, S. Phillips, and D. Sawyer, "Laser trackers for large-scale dimensional metrology: A review," Prec Eng, vol. 44, pp. 13-28, 2016.
[18] V. Collado, A. Saenz, J. Gonzalez, and J. Astorga, "ROPTALMU – A New Concept of Crawling Portable Robotic System for Wing Spars Drilling," SAE Technical Paper, no. 2009-01-3158, 2009.
[19] R. DeVlieg and T. Szallay, "Applied Accurate Robotic Drilling for Aircraft Fuselage," SAE Int J Aerospace, vol. 3, no. 1, pp. 180-186, 2010.
[20] H. Yang, S. Krut, C. Baradat, and F. Pierrot, "A new concept of self-reconfigurable mobile machining centres," IEEE/RSJ Int Conf Intelligent Robots and Systems, pp. 2784-2791, 2010.
[21] Z. Wang and P. G. Maropolous, "Real-time error compensation of a three-axis machine tool using a laser tracker," Int J Adv Manuf Technol, vol. 69, no. 1, pp. 919-933, 2013.
[22] M. Uekita and Y. Takaya, "On-machine dimensional measurement of large parts by compensating for volumetric errors of machine tools," Prec Eng, vol. 43, pp. 200-210, 2016.
[23] Electroimpact Inc., https://www.electroimpact.com/ (accessed: June 13, 2017)
[24] Faro, Cirrus Aircraft Utilizes FARO Laser Tracker for Robot Calibration, http://www.faro.com/news-events/case-studies (accessed: June 13, 2017)
[25] H. Zhang, J. Wang, G. Zhang, Z. Gan, Z. Pan, H. Cui, and Z. Zhu, "Machining with flexible manipulator: toward improving robotic machining performance," Proc. IEEE/ASME International Conference on Advanced Intelligent Mechatronics (AIM), 2005.
[26] E. Abele, M. Weigold, and S. Rothenbcher, "Modeling and identification of an industrial robot for machining applications," CIRP Annals – Manufacturing Technology, vol. 56, no. 1, pp. 387-390, 2007.
[27] J. Wang, H. Zhang and Z. Pan, "Machining with flexible manipulators: Critical issues and solutions," INTECH Open Access Publisher, 2006.
[28] L. Cen, S. N. Melkote, J. Castle, H. Appelman, "A Wireless Force Sensing and Model Based Approach for Enhancement of Machining Accuracy in Robotic Milling." IEEE/ASME Trans. Mechatronics, vol. 21, no. 5, pp. 2227-2235, 2016.
[29] S. Ibaraki and W. Knapp, "Indirect measurement of volumetric accuracy for three-axisand five-axis machine tools: a review," Int J Autom Technol, vol. 6, no. 2, pp. 110-124, 2012.
[30] MA1900 Datasheet, Yaskawa Electric Corp., http://www.motoman.com/ (accessed: Apr. 1, 2016)
[31] Laser Tracker ION Techsheet, Faro, http://www.faro.com/ (accessed: Apr. 1, 2016)
[32] D. Huo, P. D. Maropoulos, and C. H. Cheng, "The Framework of the Virtual Laser Tracker – A Systematic Approach to the Assessment of Error sources and Uncertainty in Laser Tracker Measurement," Proc. the 6th CIRP-Sponsored Int. Conf. on Digital Enterprise Technology, pp. 507-523, 2010.
[33] P. L. Teoh, B. Shirinzadeh, C. W. Foong, and G. Alici, "The measurement uncertainties in the laser interferometry-based sensing and tracking technique," Measurement, vol. 32, no. 2, pp. 135-150, 2002.
[34] H. Schwenke, M. Franke, J. Hannaford, and H. Kunzmann, "Error mapping of CMMs and machine tools by a single tracking interferometer," CIRP Ann Manuf Technol, vol. 54, no. 1, pp. 475-478, 2005.